Journal of Visualization, Vol. 10, No. 4 (2007)367-379

Regular Paper

Time-Resolved PIV Investigation on the Unsteadiness of a Low Reynolds Number Confined Impinging Jet

Kim, K. C.*[1], Min, Y. U.*[1], Oh, S. J.*[1], An, N. H.*[2], Seoudi, B.*[2], Chun, H. H.*[2] and Lee, I.*[3]

*1 School of Mechanical Engineering, Pusan National University, San 30, Jangjeon-dong, Geumjeong-gu, Busan 609-735, Republic of Korea.
*2 Department of Naval Architecture and Ocean Engineering, Pusan National University, San 30, Jangjeon-dong, Geumjeong-gu, Busan 609-735, Republic of Korea.
*3 Advanced Ship Engineering Research Center (ASERC), Pusan National University, San 30, Jangjeon-dong, Geumjeong-gu, Busan 609-735, Republic of Korea.

Received 26 March 2007
Revised 4 June 2007

Abstract : The flow characteristics in a confined slot jet impinging on a flat plate were investigated in low Reynolds number regime by using time-resolved Particle Image Velocimetry technique. The jet Reynolds number was varied from 404 to 1026, where it is presumed that the transient regime exists. We found that the vortical structures in the shear layer are developed with increase of Reynolds number and that the jet becomes remains steady at the Reynolds number of 404. Vortical structures and their temporal evolution are verified and the results were compared with previous numerical studies.

Keywords : Impinging jet, Confined slot jet, Reynolds Number, Strouhal number, POD analysis.

1. Introduction

Impinging jet flow is characterized by relatively small pressure drop as well as high heat/mass transfer rate. Those features of impinging jet flow have enabled application to cool such various components as turbine blade, combustor wall, electronic chips, etc. Most previous researches have been focused on the estimation of the flow characteristics in high Reynolds number regime. Investigations have been made of the influence of various geometric parameters such as the distance between nozzle and flat plate, shape of the jet exit nozzle, jet impinging angle on the flow field and heat transfer characteristics. Along with the rapid progress of electrical devices, however, the study on confined impinging jet in low Reynolds number has been issued. Sparrow and Wong (1975) investigated heat transfer characteristics in the jet impingement region using naphthalene sublimation technique and the analogy between heat transfer and mass transfer. Another experimental research was performed by Beitelmal et al. (2000), who identified the influence of the impingement angle on the heat transfer characteristics.

Recently, the transition of the jet flow from steady regime to unsteady regime induced by the behavior of vortex pair has been simulated in numerical researches. Particularly in case of electronics packaging cooling flow, confined jet flow between the upper nozzle plane and the impingement surface shows a complicated flow topology where the free jet behavior is associated with the flows along the upper and lower surfaces. Chung et al. (2002) reported the fallacy of the Reynolds analogy

through the numerical simulation of low Reynolds number (Re = 300 ~ 1,000) confined slot impinging jet. Numerical simulation by Chiriac and Ortega (2002) demonstrated a transition from the steady to unsteady regime with increasing Reynolds number in the confined slot impinging jet. In the unsteady regime, it was shown that the symmetry of the flow is broken due to the vortical motion in the jet before the flow impinges.

The understanding of the unsteady behavior is of great importance in the proper design of cooling system of the electronic packaging. However, the literature survey reveals that the experimental research regarding this phenomenon has been scarcely reported. Recently, time-resolved PIV technique is widely used to delineate dynamic behavior of unsteady flows (Bi et al., 2003; Vétel et al., 2006). In this study, the unsteady behavior of the impinging jet flow was analyzed by using time-resolved PIV technique and vortical structure and their interactive evolution structures are identified by means of a POD (proper orthogonal decomposition) analysis.

2. Experimental Methodology

2.1 Impinging Jet and PIV Setup

The schematic diagram of the confined impinging slot jet and the coordinate system are shown in Figs. 1 and 2, respectively. The width (W) of the jet exit was 10 mm and the height (H), length (L) and depth (D) of the confinement channel were 50 mm, 250 mm and 100 mm, respectively. De-ionized water in the reservoir is driven by an inverter-controlled pump to flow through a flow meter and a diffuser. The flow rate of the water was adjusted by means of the inverter and flow meter to maintain predetermined Reynolds number of the flow. A two-dimensional contraction shown in Fig. 1(b) was installed downstream of the diffuser to control flow quality. The contraction exit was placed along the midplane of the confinement channel to form the jet exit slot. As seen in Fig. 2, the x-direction corresponds to the jet-transverse direction, while the y-axis to the jet-streamwise direction.

The time-resolved PIV system (Dantec Dynamics) consisted of high repetition rate Nd:YAG laser, high-speed CMOS camera and synchronizer. The illuminating laser was a Lee diode-pumped Nd:YAG laser (LDP-100MQG) with output wavelength of 532 nm, variable repetition rate from 10 Hz to 20 kHz, and pulse energy of 11 mJ. The high-speed camera was a 10-bit resolution IDT CMOS camera (X-Stream XS-3) with a maximum frame rate of 660 Hz, a pixel resolution of 1,280 × 1,024 and internal flash memory of 1GByte. This memory capacity allowed successive acquisition of 253 frame pairs with the maximum frame resolution of 1,280 × 1,024 pixels. Hollow glass beads with a diameter of 10μm had been added in the water reservoir prior to the measurement.

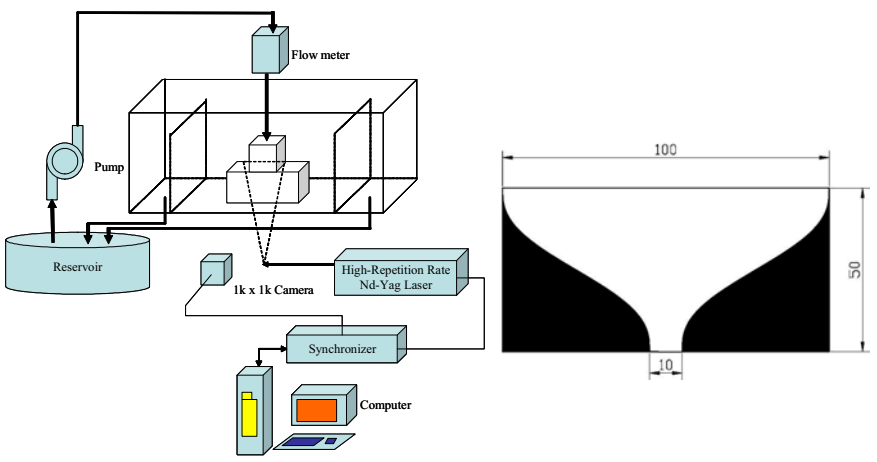

Fig. 1. Schematic diagram of experimental apparatus; (a) PIV system setup, (b) contraction type nozzle.

Experiments were conducted by varying Reynolds numbers of 400, 800 and 1,000, which was defined by the average jet exit velocity Vj and jet exit width W. Table 1 summarizes the corresponding average jet exit velocities, delay times between particle image pair and the frame rates for the respective Reynolds numbers. The measurement area was located in the central xy-plane with the field of view being 72 mm × 50 mm ($-3.6 \le x/W \le 3.6, 0 \le y/W \le 5$). For each measurement, 253 particle image pairs were recorded and transferred to the personal computer. The corresponding time history of the particle displacement was then calculated using cross-correlation algorithms. The interrogation window was 32 × 32 pixels in size and overlapped 50 %. The resulting spatial resolution was 0.0930W and 0.133W in the x- and y-directions, respectively.

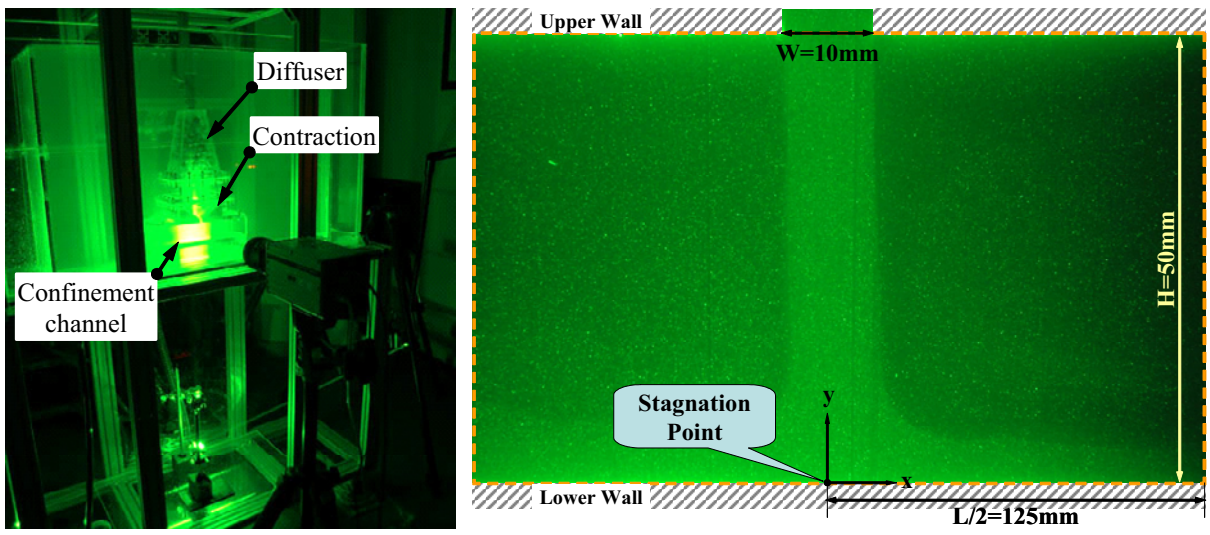

Fig. 2. Photos of experimental facility; (a) overall setup, (b) measuring area and coordinate system.

Table 1. Measurement conditions.

Re	V_j (m/s)	Delay time (μs)	Frame rate (Hz)	Measurement duration (s)
404	0.0383	1,000	50	5.06
821	0.0780	1,000	50	5.06
1,026	0.0974	1,000	50	5.06

2.2 Proper Orthogonal Decomposition

The Proper Orthogonal Decomposition (hereinafter called as POD) is a well-known technique determining an optimal basis for the reconstruction of a data set. Since introduced by Karhunen (1946), this technique has been extensively employed for the extraction and identification of the coherent structures (Berkooz et al., 1993). The basis function obtained from POD analysis of a spatial function represents a dominant structure. For a spatio-temporal velocity field $u(\vec{x},t)$, POD determines orthonormal functions $\varphi_j(\vec{x})$, $j = 1, 2, \cdots$, such that the projection of the velocity field onto the first n functions $\hat{u}(\vec{x},t) = \sum_{j=1}^{n} a_j(t)\varphi_j(\vec{x})$ minimizes the square error of the projection E, defined by $E = \left\langle \left\| u(\vec{x},t) - \sum_{j=1}^{n} a_j(t)\varphi_j(\vec{x}) \right\|^2 \right\rangle$. The functions $\varphi_j(\vec{x})$ are obtained by solving the integral equation

$$\int R(\vec{x},\vec{x}^*)\varphi(\vec{x}^*)d\vec{x}^* = \lambda\varphi(\vec{x})$$

where $R(\vec{x},\vec{x}^*)=\langle u(\vec{x})u(\vec{x}^*)\rangle$ is the autocorrelation of the velocity. The above equation is again an eigenvalue problem with the integration variable being $\vec{x}^*$. Solving this equation gives n eigenfunctions $\varphi_j(\vec{x}), j=1,2,\cdots,n$. For a function with two-dimensional spatial dependence, direct numerical calculation of the above integral equation requires considerable amount of calculation time. The method of snapshots proposed by Sirovich (1987), leads to a dramatic saving in computational effort in computing the eigenfunctions. In this study, the method of snapshots has been employed.

3. Results

3.1 Overall Flow Characteristics

The initial conditions of the jet at exit have significant influence on the downstream development of the shear layer and the consequent transition between steady and unsteady regimes. As seen in Fig. 3, both the mean velocity as well as the rms velocity shows non-uniform and asymmetric distribution across the jet exit plane ($-0.5 \le x/W \le 0.5$). This is attributed to an excessive streamline curvature near the jet exit. Moreover, it is found that the asymmetrical velocity distribution results in deflected jet impingement. This is attributed to the limitations of the present experimental setup such as short contraction, restricted length of the whole circuitry. However, the initial conditions remain essentially unchanged with increasing Reynolds number.

Figures 4 and 5 represent the comparison between the time-mean flow field and the instantaneous flow field with increasing Reynolds number, along with the contour plots of turbulence intensity. For $Re = 404$ (Fig. 4), the instantaneous flow field is almost the same as the time-mean flow field. The lack of lateral growth of the shear layer in Fig. 4(c) implies that there is no vortex formation. It is found that steady flow regime is established for this low Reynolds number. For $Re = 821$, the shear layer near impingement point ($y/W < 1.0$) appears to roll-up. For larger Reynolds number of $Re = 1{,}026$ (Fig. 5), the formation of vortical structure is more pronounced, which is also evidenced by the lateral growth of the shear layer. It is now seen that the transition from steady to unsteady regime occurs below $Re = 821$. This phenomenon is comparable to the transition at $Re = V_j W/\nu = 325$ in Chiriac and Ortega (2002). Furthermore, vortices are formed symmetrically with respect to the jet centerline (see Fig. 5(b)), which is contrary to the asymmetric, staggered vortex formation reported by Chiriac and Ortega (2002). This discrepancy is attributable to the difference in the boundary conditions, *e.g.*, finite velocity gradient across the initial shear layer associated with non-uniform jet exit velocity profile in the present study.

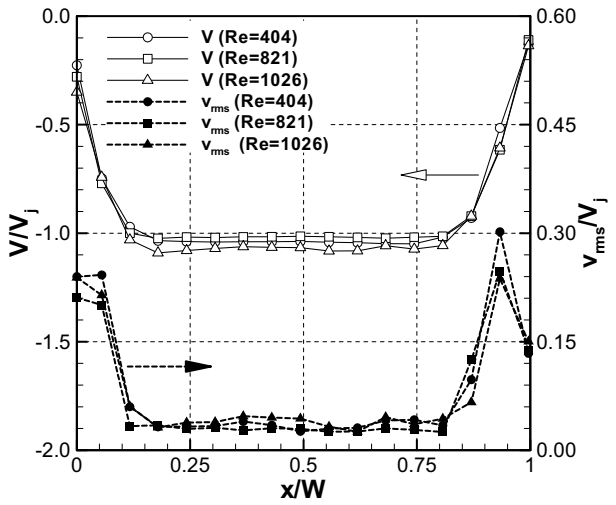

Fig. 3. Distribution of mean and rms jet exit velocity normalized by average jet exit velocity V.

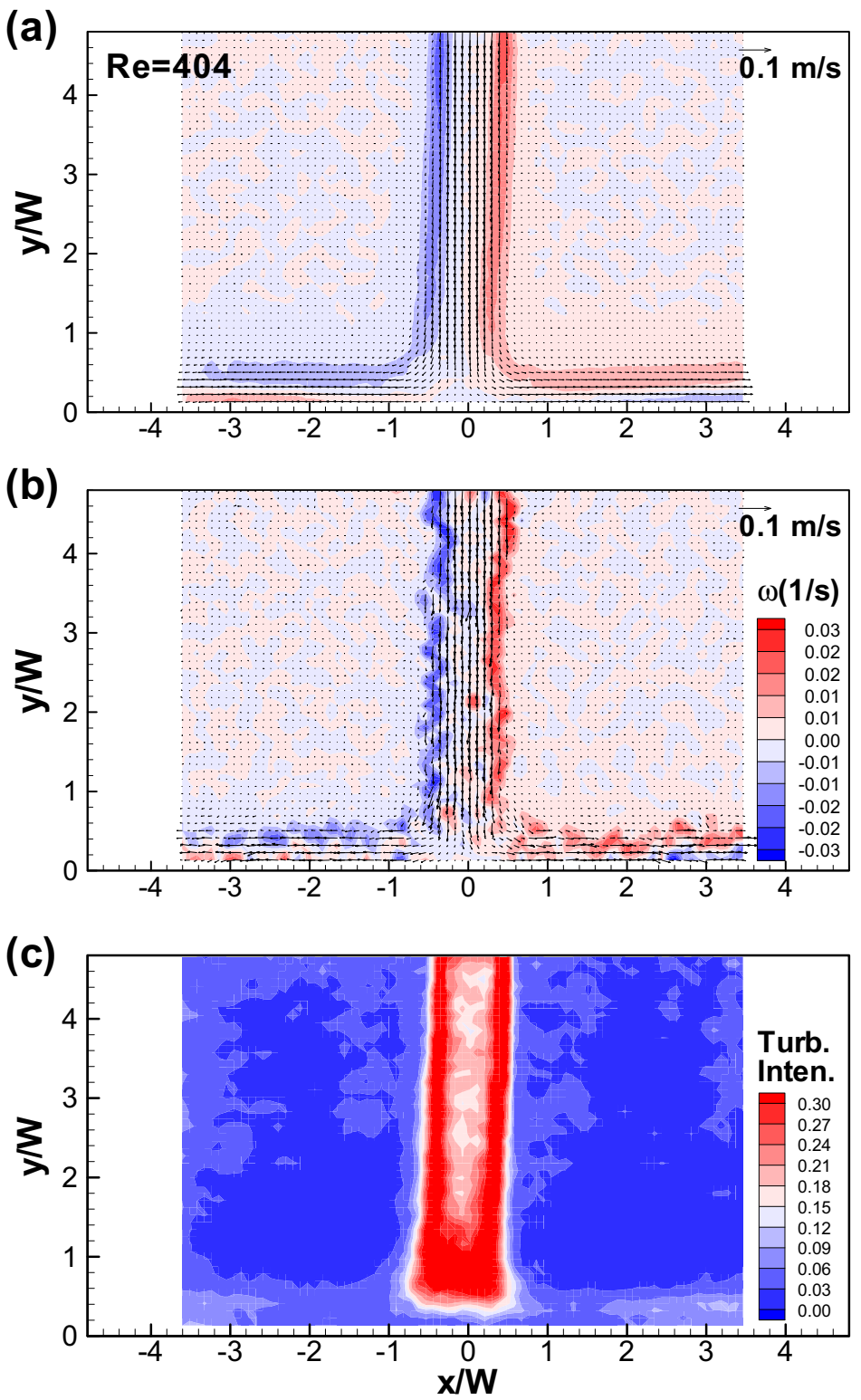

Fig. 4. Comparison between time mean and instantaneous velocity field at Re = 404; (a) time mean velocity vector plot and vorticity contour plot, (b) instantaneous velocity vector plot and vorticity contour plot, (c) contour plot of turbulence intensity.

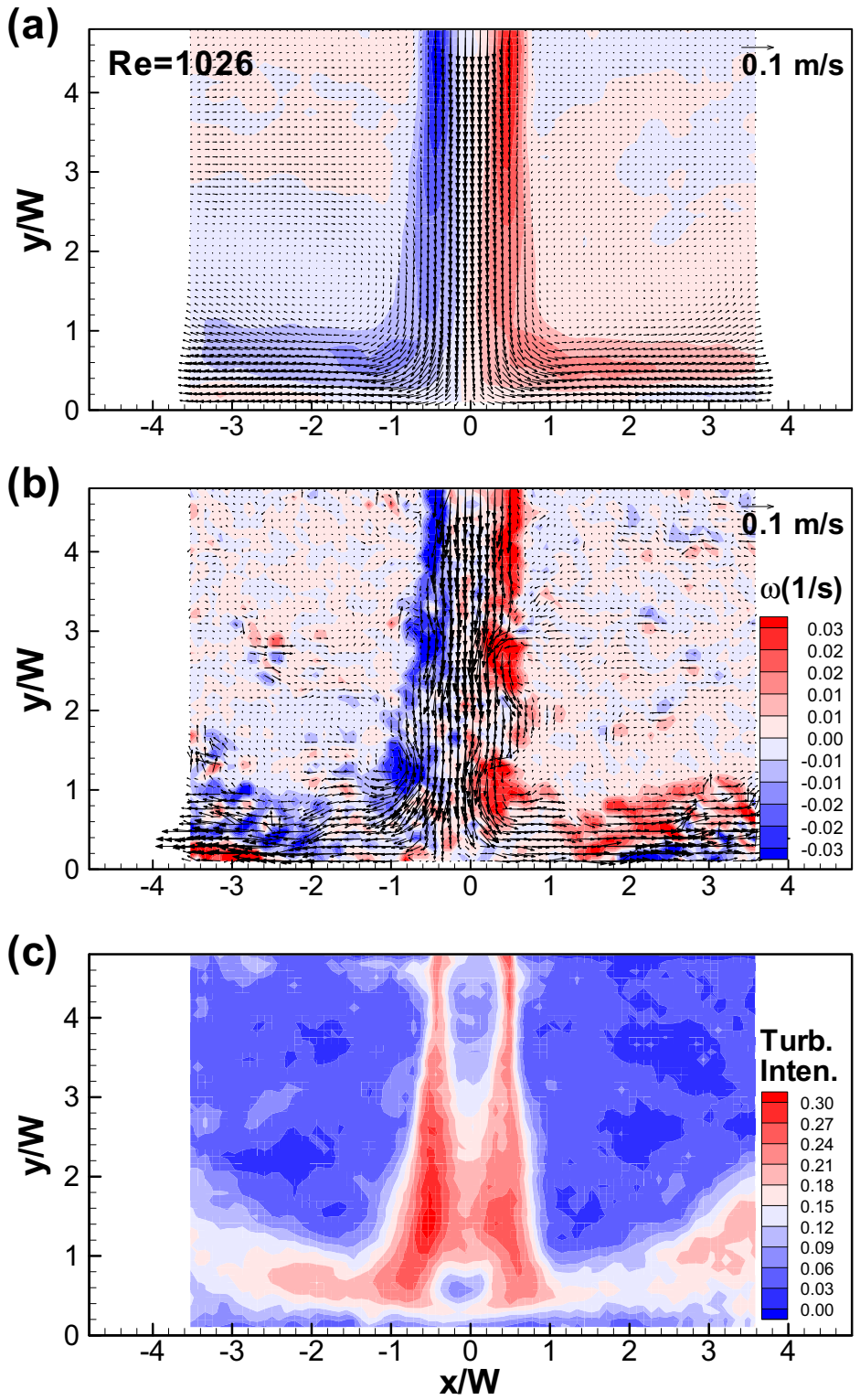

Fig. 5. Comparison between time mean and instantaneous velocity field at Re = 1026; (a) time mean velocity vector plot and vorticity contour plot, (b) instantaneous velocity vector plot and vorticity contour plot, (c) contour plot of turbulence intensity.

3.2 POD Analysis

In POD analysis, the eigenvalue represents the energy of each eigenmodes. Figure 6 demonstrates such energy distribution the corresponding cumulative energy sum with respect to the mode number at various Reynolds numbers. It is clear that most of the flow energy is concentrated on a few fundamental eigenmodes for all the Reynolds numbers considered. A closer inspection of Fig. 6 indicates that the higher Reynolds number, the more flow energy concentrated on the fundamental modes. For instance, the ratio of the energy of the first six eigenmodes to the total flow energy is 90.6 % at $\mathrm{Re} = 404$, while the ratio becomes 95.0 % at $\mathrm{Re} = 1{,}026$. This implies that the flow becomes more identified with lower dimensional spatial structures as the Reynolds number increases.

Comparison between the instantaneous PIV measurement results and the corresponding POD reconstruction from 20 eigenmodes is given in Fig. 7. Eight successive frames spaced with constant time interval of 1/8T are sampled for both PIV measurements (Fig. 7(a)) and POD reconstruction (Fig. 7(b)). Here, T was chosen to correspond roughly to the vortex formation period, i.e., $TV_j/H \approx 1.70$. The two results show close resemblance to each other, which is a manifestation of the validity for the present POD analysis.

The velocity vector plots and the contour plots of vorticity of the POD eigenmodes up to the fifth mode, along with the time histories of the corresponding POD coefficients are given in Figs. 8 and 9 for $\mathrm{Re} =$ 404 and 1,026. For every POD analysis result, the first eigenmode corresponds to time-mean velocity field. For $\mathrm{Re} = 404$ (Fig. 8), the eigenmodes higher than the first mode resemble one another without any notable spatial structures. The POD coefficients ($a_i(t), i \geq 2$) indicate trivial noisy characteristics. These observations are consistent with the above-mentioned reasoning that steady flow regime is established for this low Reynolds number.

The existence of coherent structures and their modal characteristics become pronounced for larger Reynolds number ($\mathrm{Re} = 1{,}026$) in Fig. 9. The fourth and fifth modes display well organized vortical structure. As described in the next section, these POD mode coefficients are dominated by the frequency of the coherent vortical structure, $fH/V_j \approx 1.7$.

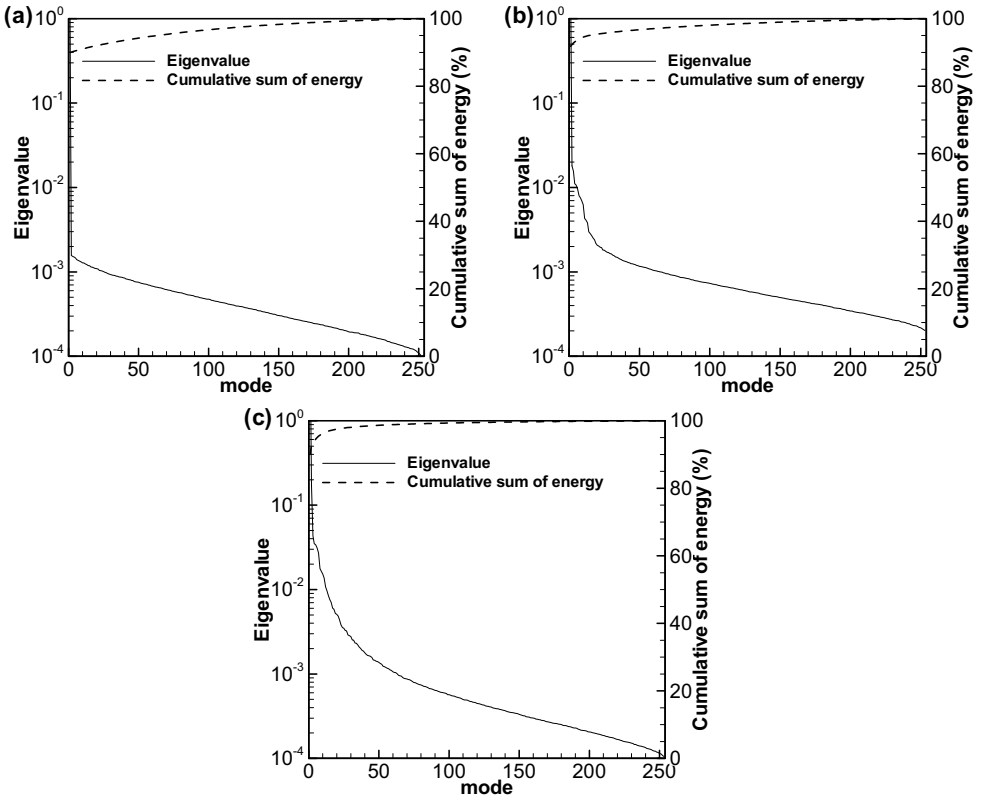

Fig. 6. Modal distributions of POD eigenvalues with varying Re; (a) Re = 404, (b) Re = 821, (c) Re = 1,026.

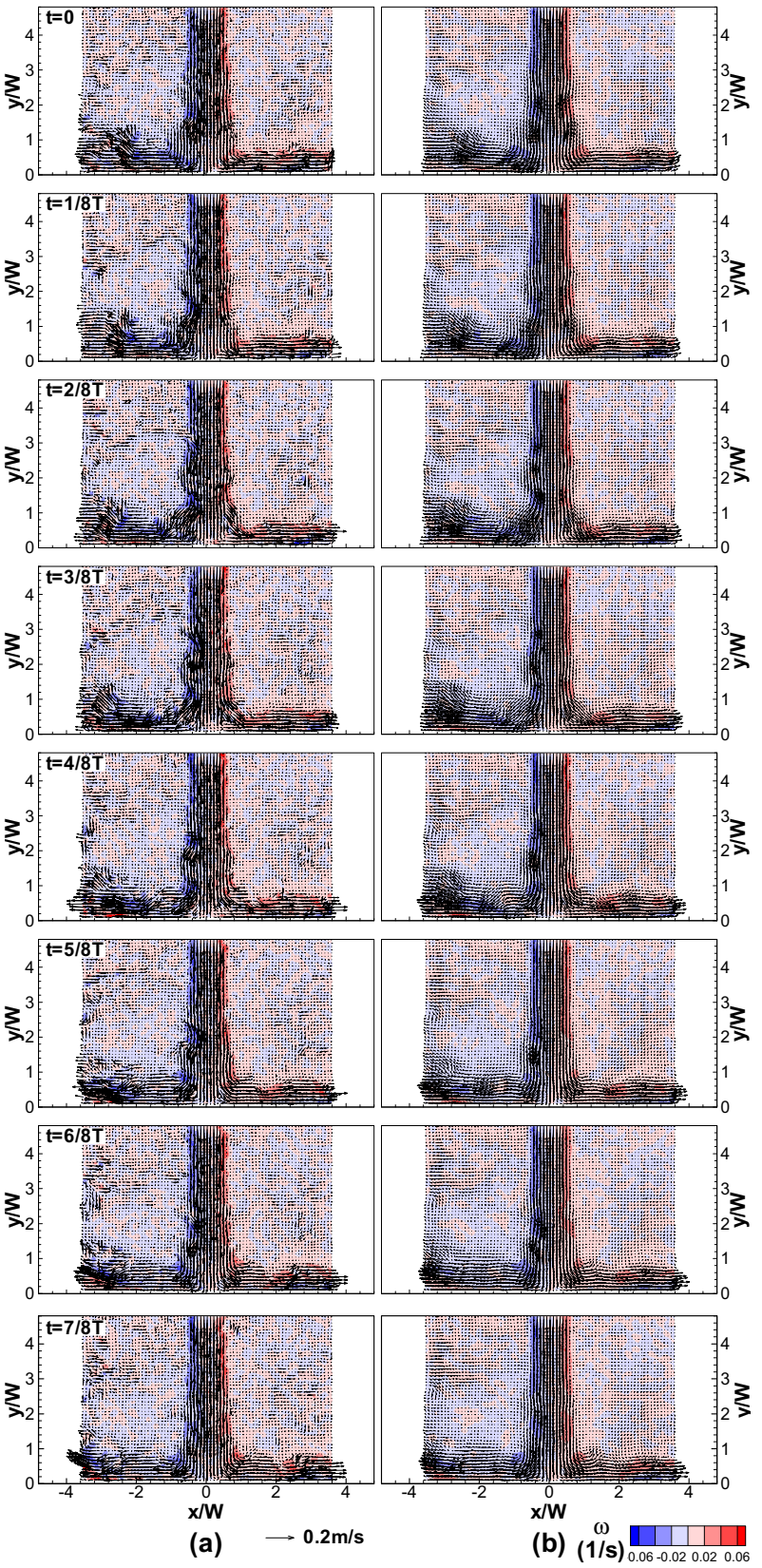

Fig. 7. Comparison of time histories of velocity vector plots and contour plots of vorticity at Re = 1,026; (a) instantaneous flow field, (b) POD reconstruction with 20 eigenmodes.

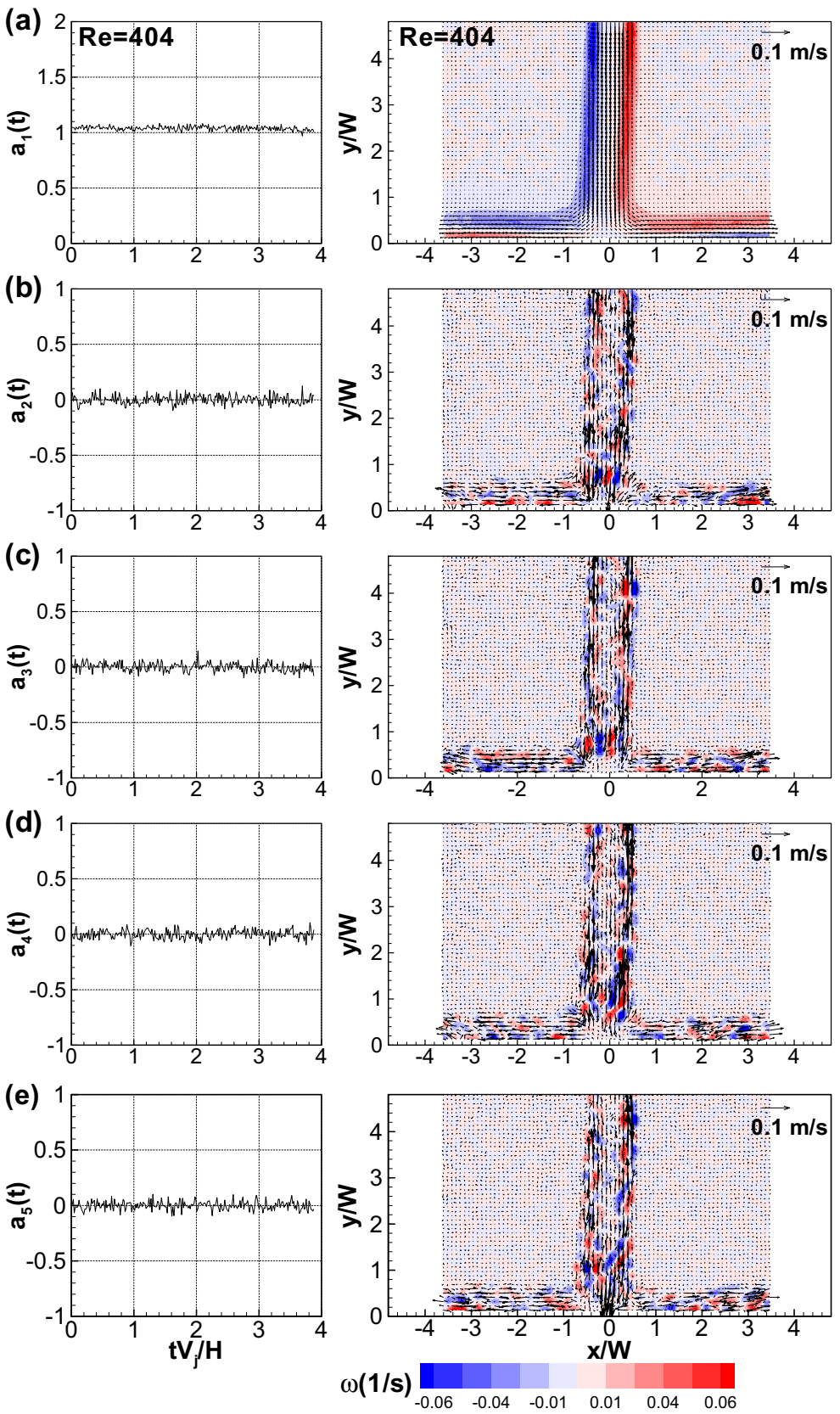

Fig. 8. Time histories of POD mode coefficients and contour plots of eigenmodes at Re = 404; (a) 1st mode, (b) 2nd mode, (c) 3rd mode, (4) 4th mode, (5) 5th mode.

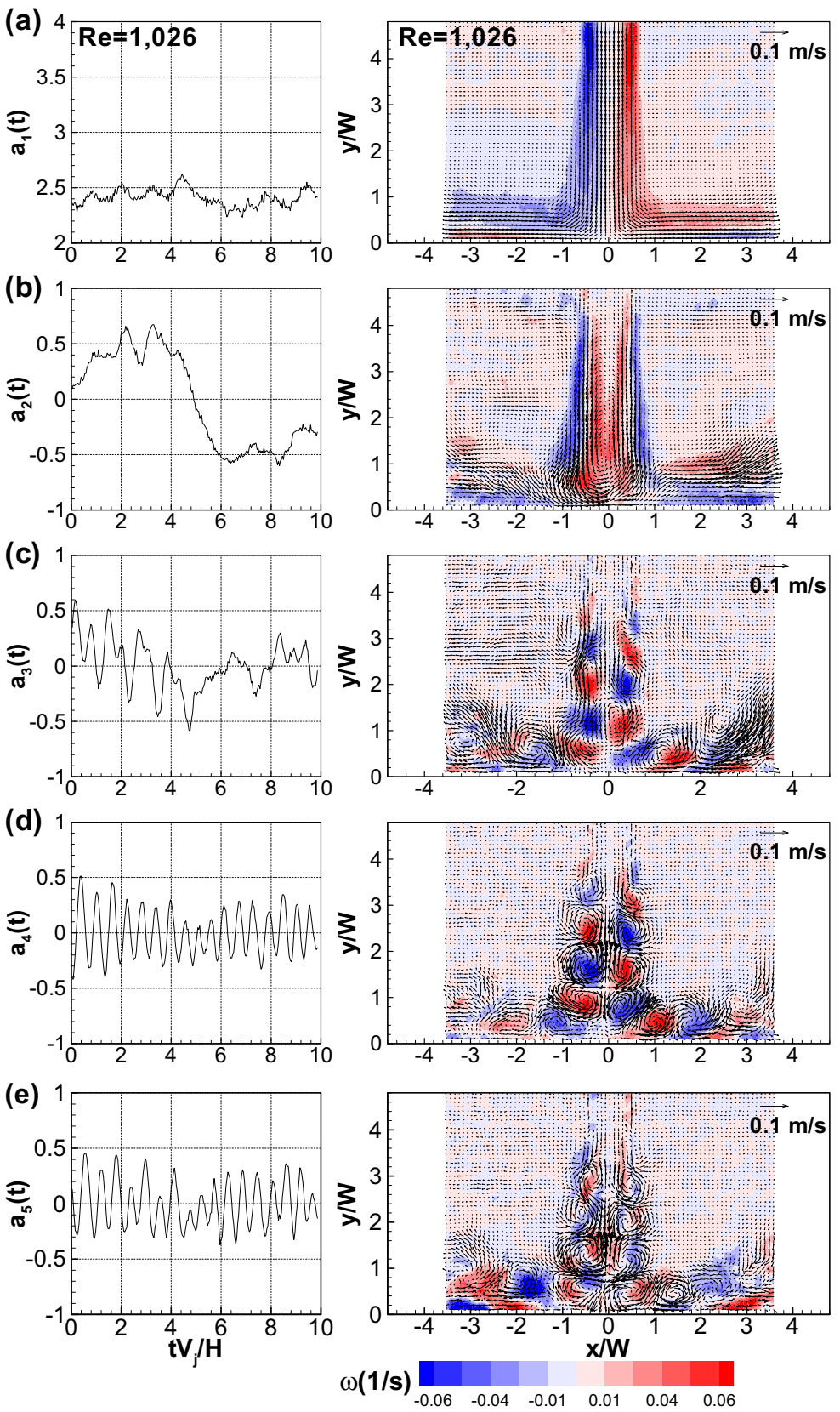

Fig. 9. Time histories of POD mode coefficients and contour plots of eigenmodes at Re = 1,026; (a) 1st mode, (b) 2nd mode, (c) 3rd mode, (4) 4th mode, (5) 5th mode.

The second mode becomes distinguished by the presence of low-frequency unsteadiness, of which nondimensional frequency $fH/V_j \approx 0.1$ is less than 1/10 of the frequency of vortical structure. A closer inspection of the real-time velocity field reconstruction using only the first and second eigenmodes demonstrates a very slow lateral flapping motion of the jet impingement. It is conjectured that this motion is associated with larger scale instability, for instance, instability pertaining to the confinement channel. The third mode shows a modulatory reaction between the lateral flapping motion (second mode) and the regular vertical structure (fourth mode). Finally, it is notable that the vortices are formed symmetrically, which is contrary to the asymmetric vortex formation in the numerical simulation of Chiriac and Ortega (2002). Instantaneous flow field as well as the reconstructed field from fundamental modes does not confirm such asymmetric, staggered vortex formation. It is not clear that the "staggered" vortex formation is intrinsic in the confined slot impinging jet flow. This is because symmetric vortex formation is evident in Chung et al. (2002). Thus, the discrepancy regarding vortex formation pattern could appropriately be attributed to the difference in the boundary conditions.

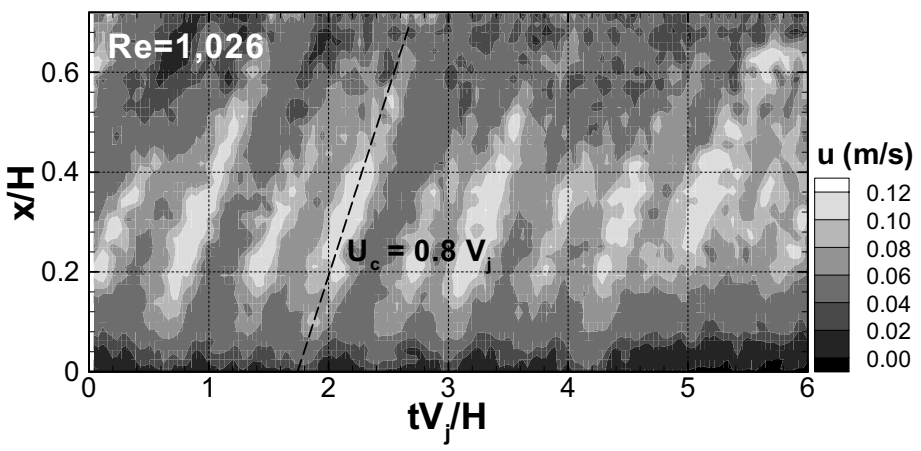

Fig. 10. Space-time contour plots of u-velocity near the wall (y/W=0.1) at Re =1,026.

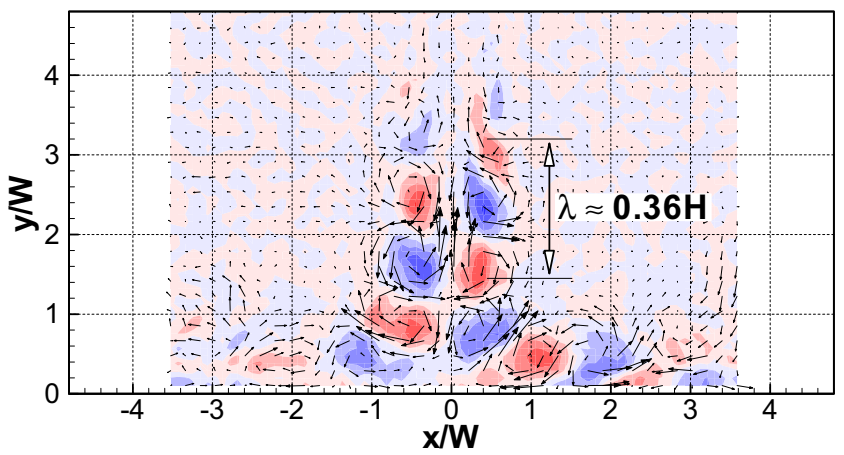

Fig. 11. Conceptual diagram of vortex formation mechanics.

3.3 Vortex Formation Mechanism

In the confined impinging jet, the characteristic frequency V_j/H, which is defined by the average jet exit velocity V_j and the height of the confinement channel H, was found to be closely related with the vortex formation frequency (Chiriac and Ortega, 2002). The nondimensional frequency of Strouhal number is consequently defined using the characteristic frequency as $St = fH/V_j$. The corresponding

vortex formation Strouhal number is then found to be $fH/V_j \approx 1.8$, which is similar to $fH/V_j \approx 2.0$ from the numerical result of Chung et al. (2002). (Note that $St = fD/V_j \approx 0.2$ with D being jet width and $H/D = 10$ in Chung et al. 2002). This value also falls within the range of other researches, $St \approx 2.3$ (Didden and Ho, 1985; Olsson and Fuchcs, 1998). The Strouhal number was shown to be $St \approx 1.1$ in case of the asymmetric vortex formation (Chiriac and Ortega, 2002). This indicates that the symmetric vortex formation frequency is roughly twice the asymmetric counterpart. Figure 10 displays a space-time contour plot of u-velocity (jet-transverse) measured in the near-wall region ($y/W = 0.1$). The convection of large-scale vortical structure is clearly found from the presence of inclined elliptical contours, the "vortex packets". The inclination of the packet corresponds to the convection velocity, which is shown to be $U_c/V_j = 0.8$ by the dashed line. The convection velocity obtained in the near-wall region after impingement is comparable to that in the vortex formation region. Thus, the frequency and the wavelength (spacing) of the coherent vortices remain essentially unchanged upon impingement. This conjecture is supported by the observation of POD eigenmodes, one of which is plotted in Fig. 11, which is a close-up view of the fourth eigenmode for $Re = 1{,}026$. It is seen that the wavelength λ – spacing between coherent vortices – is found to be $\lambda \approx 0.36H$. From the above information, the vortex formation frequency is given as $f = U_c/\lambda = 0.8V_j/0.36H = 2.2V_j/H$. Therefore, the corresponding Strouhal number becomes 2.2, which is comparable to the measured value of 1.8. This reasoning is basically the same as that by Chiriac and Ortega (2002) except the symmetric vs. asymmetric vortex formation. Thus, it can be concluded that the vortex formation is basically governed by a feedback mechanism between the jet exit and the impinging wall.

4. Conclusion

Experimental investigations have been made of the unsteady behavior of a confined slot jet impinging on a flat plate using time-resolved PIV (Particle Image Velocimetry) technique. Transition from steady to unsteady regime does not occur up to $Re = 404$. For larger Reynolds numbers, symmetric vortices are formed in the jet shear layer and the vortex formation region becomes nearer to the jet exit. The vortex formation frequency was found to scale with the characteristic frequency defined by the jet exit velocity and the height of the confinement channel.

Acknowledgement

This research was sponsored by the Brain Korea 21 program of MOE and by the ERC program (Advanced Ship Engineering Research Center) of MOST/KOSEF.

References

Bi, W., Sugii, Y., Okamoto, K. and Madarame, H., Time-resolved proper orthogonal decomposition of the near-field flow of a round jet measured by dynamic particle image velocimetry, Measurement Science and Technology, 14 (2003), L1~L5.

Beitelmal, A. H., Saad, M. A. and Patel, C. D., The Effect of Inclination on the Heat Transfer Between a Flat Surface and Impinging Two-dimensional Air Jet, Int. J. Heat Fluid Flow, 18 (2000), 597~605.

Berkooz, G., Holmes, P. and Lumley, J., The proper orthogonal decomposition in the analysis of turbulent flows, Ann. Rev. Fluid Mech., 25 (1993), 539~575.

Chiriac, V. C. and Ortega, A., Numerical Study of Unsteady Flow and Hear transfer in a Transitional Confined Slot Jet Impinging on an Isothermal Surface, Int. J. Heat Mass Transfer, 45 (2002), 1237~1248.

Chung, Y. M., Luo, K. H. and Sandham, N. D., Numerical Study of Momentum and Heat Transfer in Unsteady Impinging Jets, Int. J. Heat Fluid Flow, 23 (2002), 592~600.

Didden, N. and Ho, C. M., Unsteady separation in a boundary layer produced by an impinging jet, J. Fluid Mech., 160 (1985), 235~256.

Karhunen, K., Zur spektraltheorie stochasticher, Annales Academiae Scientiarum Fennicae Series A, 1 (1946), 34.

Olsson, M. and Fuchs, L., Large eddy simulations of a forced semiconfined circular impinging jet, Phys. Fluids, 10-2 (1998), 476~486.

Sirovich, L., Turbulence and the dynamics of coherent structures, Quarterly of Applied Mathematics, 45-3 (1987), 561~590.

Sparrow, E. M. and Wong, T. C., Impingement Transfer Coefficients due to Initially Laminar Slot Jets, Int. J. Heat Mass Transfer, 18-5 (1975), 597~605.

Vétel, J., Farinas, M.-I., Garon, A. and Pelletier, D. Characterization of a Diffuser Flow by Time-Resolved PIV, Journal of Visualization, 9-2 (2006), 219~226.

Author Profile

Kyung Chun Kim: He is a Professor in the School of Mechanical Engineering of Pusan National University and the director of the Brain Korea 21 project team for "Amenity Control and Energy Saving for Air-Conditioning System". Prof. Kim obtained his Ph.D. from KAIST (Korea Advanced Institute of Science and Technology), Korea, in 1987. His research interests include: turbulence measurements and mathematical modeling, turbulent convective heat transfer, microprocessor application in thermal-fluid system, wind Engineering and turbulent dispersion in atmospheric boundary layer.

Young Uk Min: He is a Ph. D student in the School of Mechanical Engineering of Pusan National University. He got his M. S. degree in the department of the mechanical engineering of Ajou University in 2002. His research topics are measurement of microflow in microdevices fabricated with MEMS technology by using Micro-PIV and his research interests include the development of measurement and control techniques in microscale devices like TIRFM(Total internal reflection Fluorescence microscopy) and blood separation using microchannels.

Sung Jin Oh: He works now as design engineer in Korea Gas Corporation. He got his M. S. degree in the School of Mechanical Engineering of Pusan National University in 2006. He now works in Korea Gas Safety Corporation(KGS), His research topics are the experimental study of the unsteady flow in a transitional confined slot jet impinging on a flat surface.

Nam Hyun An: He is an M. S. student in the department of Naval Architecture and Ocean Engineering of Pusan National University. He got his B. S. degree in the same department in 2000. He worked in Hyundai Heavy Industries Co. Ltd. from 2000 to 2004. His research topics are the skin friction reduction of turbulent boundary layer using outer-layer blades and flow visualization using PIV (Particle Image Velocimetry).

Basel Seoudi: He is a Ph. D. student in the Department of Naval Architecture and Ocean Engineering of Pusan National University. He works as Teaching Assistant in marine engineering department of Arab Academy for Science, Technology and Maritime Transport (AASTMT), Alexandria, Egypt since 1999 till now. He obtained his 2nd Marine Engineer Certificate from (AAST) in 2000. He obtained his M. Sc. from (AASTMT) in 2003. His study interests include drag reduction, compliant coating, flow visualization and PIV (Particle Image Velocimetry).

Ho Hwan Chun: He is a Professor in the Department of Naval Architecture & Ocean Engineering and director of Advanced Ship Engineering Research Center (ASERC). Prof. Chun obtained his Ph.D from University of Glasgow, UK., in 1988. His research interests include: ship hydrodynamics, computational fluid dynamics, high speed ship designs, towing tankery problems, fluid mechanics and drag reduction.

Inwon Lee: He is an Assistant Professor in the Advanced Ship Engineering Research Center (ASERC) of Pusan National University. Prof. Lee obtained his Ph.D. from KAIST (Korea Advanced Institute of Science and Technology), Korea, in 2000. His research interests include: drag reduction, turbulent flow control, flow visualization and PIV (Particle Image Velocimetry).